RSC Advances

ROYAL SOCIETY OF CHEMISTRY

www.rsc.org/advances

TOC

Fabrication of SiO_2 incorporated ordered mesoporous TiO_2 composite films as functional Pt supports for photo-electrocatalytic methanol oxidation

X. L. Fan,[a] C. X. Zhang[b], H. R. Xue,[a] H. Guo,[a] L. Song[a] and J. P. He [*a]

[a]College of Materials Science and Technology, Jiangsu Key Laboratory of Materials and Technology for Energy Conversion, Nanjing University of Aeronautics and Astronautics, 210016 Nanjing, PR China.
[b]Jiangsu Key Laboratory of Advanced Structural Materials and Application Technology, College of Materials Engineering, Nanjing Institute of Technology, 211167 Nanjing, PR China.
* Corresponding author. Tel: +86 25 52112900; Fax: +86 25 52112626.
E-mail address: jianph@nuaa.edu.cn (J. P. He)

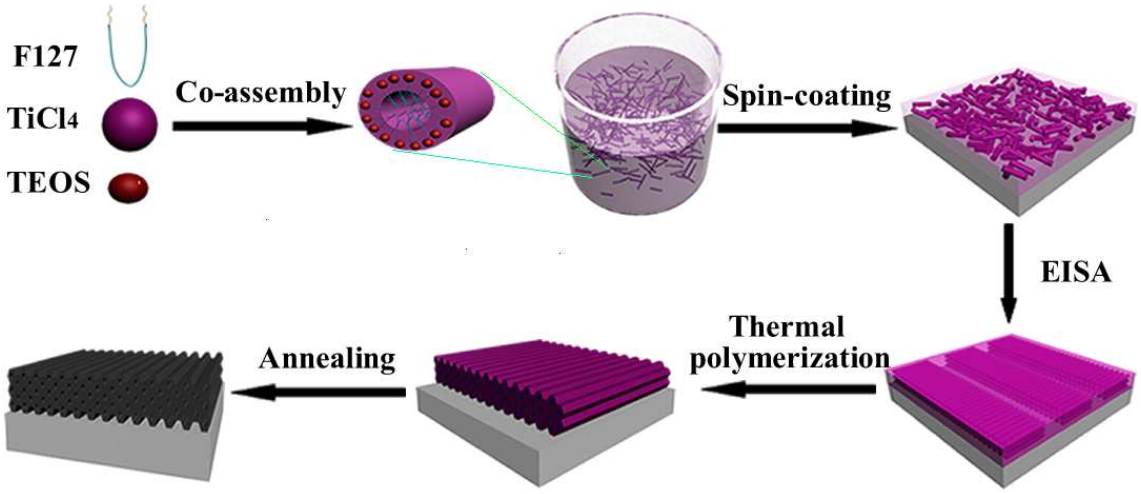

SiO_2 incorporated ordered mesoporous TiO_2 composite films were fabricated as active support for methanol oxidation and excellent photoelectrocatalytic activity was obtained, showing great potential application prospect.

RSC Advances

ARTICLE

Fabrication of SiO_2 incorporated ordered mesoporous TiO_2 composite films as functional Pt supports for photo-electrocatalytic methanol oxidation

Received 00th January 20xx,
Accepted 00th January 20xx

DOI: 10.1039/x0xx00000x

www.rsc.org/

X. L. Fan,[a] C. X. Zhang[b], H. R. Xue,[a] H. Guo,[a] L. Song[a] and J. P. He [*a]

SiO_2 incorporated ordered mesoporous TiO_2 composite films (TS) have been fabricated onto the FTO glass through a sol-gel progress, applied as Pt catalyst support materials for Direct Methanol Fuel Cells. In this work, we investigate the effects of different SiO_2 doping content and calcination temperature on the structure and corresponding properties of the resulting TiO_2-SiO_2 films. Characterization techniques including X-ray diffraction (XRD), fourier transforming infrared spectrum (FT-IR), field emission scanning electron microscopy (FESEM) and transmission electron microscopy (TEM) are used to characterize the synthesized films. Potentiostatic pulse electrodeposition is employed to deposit Pt on the ordered mesoporous TiO_2-SiO_2 films. Results reveal that the films possess 2D hexagonal mesoporous structure and Si element is uniformly dispersed in the TiO_2 matrix. Moreover, the ordered mesoporous Pt/TiO_2-SiO_2 film electrode calcinated at 500°C with 7.5 wt % of SiO_2 shows enhanced catalytic activity for methanol oxidation, due to the high photoelectric response and the special synergetic effects between Pt and TiO_2-SiO_2 films under UV illumination.

Introduction

Generally, metal platinum or palladium together with their alloy catalysts dispersed on carbon support are currently most applied for catalytic methanol oxidation in direct methanol fuel cells (DMFCs).[1-5] However, practical applications of these catalysts have been severely limited due to weak dispersion and easy agglomeration of metal nanoparticles introduced by exfoliation of supporting carbon materials[6-8] and CO poisoning effect of noble metal platinum[9, 10] under DMFCs work conditions. Many efforts have been devoted to exploring suitable catalyst support materials. One efficient strategy is to coupling noble metal or alloy with metal oxides (e.g., TiO_2[11], WO_3[12, 13], ZnO_2[14], CeO_2[15, 16]) instead of carbon materials. The resulting metal oxides supported catalysts can efficiently alleviate CO positioning effect[14] and thereby promote the catalytic performance and durability of catalysts.[17] Of all the candidates, the n-type semiconductor TiO_2 attracts the most attentions due to its excellent chemical inertness, low cost, non-toxicity, and relatively high photocatalytic activity[18] under light irradiation, making it the most promising support material.[19] Moreover, under UV illumination, TiO_2 is essentially prone to give the photoexcited electrons and holes,[20, 21] which can migrate to the surface and subsequently induce redox reactions. Photo-generated holes in the valence band together with their reaction products (e.g., •OH) with H_2O have strong oxidizing ability, which can make for methanol oxidation. Nevertheless, as a wide band-gap semiconductor, its commercialization applications still suffer from some intrinsic defects such as the poor electric conductivity,[22] poor solar energy harvesting ability and high charge recombination rate.[23] To overcome these limitations, effective strategies should be explored extensively to adjust the structure, morphology and crystallinity of TiO_2.

It has been identified that Schottky barrier can be formed at the metal semiconductor interface when Pt nanoparticles are dispersed on TiO_2, which could facilitate the interfacial electrons transfer from TiO_2 to Pt, promote charge carriers separation, and subsequently decrease the hole-electron recombination.[24] Meanwhile, the whole Pt/TiO_2 catalysts can improve the solar energy utilization since Pt particles exhibit full spectrum absorption.[25, 26] On the other hand, the performance of catalysts is determined to a great extent by their textural properties. Fabrication of ordered mesoporous TiO_2 film supports with uniform pore channels and rather high surface areas can significantly facilitate fast mass transportation,[27] enhance the adsorption of reactants, make for nano-sized Pt catalysts deposition,[28] and ultimately increase accessible reactive sites on the catalyst surface. What's more, the porous structure can contribute to the transfer of photogenerated carriers, and hence slow down the recombination ratio of electrons and holes,[29] which enhances the whole catalytic efficiency. Based on this consideration, silica was introduced into the titania framework in order to

[a] College of Materials Science and Technology, Jiangsu Key Laboratory of Materials and Technology for Energy Conversion, Nanjing University of Aeronautics and Astronautics, 210016 Nanjing, PR China. E-mail address: jianph@nuaa.edu.cn; Tel: +86 25 52112900; Fax: +86 25 52112626.
[b] Jiangsu Key Laboratory of Advanced Structural Materials and Application Technology, College of Materials Engineering, Nanjing Institute of Technology, 211167 Nanjing, PR China.

prepare the high crystallized TiO_2 material with well-defined mesoporous structure concurrently at high temperature heat treatment.

Silica is a favourable participant as stabilizer due to its high mechanical resistance, preferable transmittance, chemical inertia and thermal stability.[30] The incorporation of SiO_2 into the ordered mesoporous TiO_2 framework may result in the composites with better thermal stabilization and textural properties without destroying the mesoporous skeletons.[31, 32] The high crystallinity of TiO_2 materials under higher thermal treatment has been found to be of critically importance to enhance the generation and migration of photogenerated carriers,[18] which can significantly improve the overall photocatalytic efficiency. Lei et al. prepared the ordered mesoporous TiO_2 thin films and the films calcined at 500 °C showed effective photogenerated cathodic protection for 304SS than that at 350 °C.[33] Nevertheless, compared with the latter, degradation of mesoscopic order still happened with the former because of high crystallization of TiO_2 frameworks.[34] We have reported fabrication of ordered mesoporous TiO_2 film as Pt supports and the film catalysts calcined at 400 °C exhibited well ordered mesoporous structure and improved catalytic activity for methanol oxidation in DMFCs with electrocatalytic and photocatalytic processes simultaneously under UV irradiation.[35,36] However, the film under higher heat treatment temperature showed crashed structure and better properties still need to be explored.

Inspired by previous research, in this work we have tried to introduce SiO_2 into ordered mesoporous TiO_2 skeletons and evaluate the effects of doping SiO_2 contents and calcination temperature on the textual and catalytic performance of the resulting catalysts. Ordered mesoporous TiO_2-SiO_2 films was synthesized through a sol-gel method with F127 as the temple, resulting in stripe-shaped mesocrope channels. Pt nanoparticles were deposited onto the TiO_2-SiO_2 films through a potentiostatic pulse electrodeposition process and the photo-electrocatalytic effects for methanol oxidation between Pt and semiconductor composites under UV irradiation were studied. Special attentions were paid to investigate the influence of mesostructural orderings and pore morphologies on the photocatalytic activity of the as-prepared Pt/TiO_2-SiO_2 films.

Experimental

Materials

Triblock copolymer Pluronic F127 (Mw = 12,600, $PEO_{106}PPO_{70}PEO_{106}$, EO = ethylene oxide, PO = propylene oxide) was purchased from Sigma–Aldrich Corporation, chloroplatinic acid (H_2PtCl_6) was purchased from Nanjing Ningshi Chemical Corporation, titanium tetrachloride ($TiCl_4$), tetraethyl orthosilicate (TEOS), potassium hydroxide（KOH）, hydrochloric acid (HCl, 37 wt%), methanol (CH_3OH), ethanol (C_2H_5OH) and acetone were purchased from Shanghai Chemical Corporation. All reagents were used as received without any further purification. Distilled water was used in all experiments.

Synthetic procedures

Synthesis of ordered mesoporous TiO_2-SiO_2 films. The mesoporous TiO_2-SiO_2 composite films were synthesized via sol-gel and coating progress. In a typical synthesis, 1.12 ml $TiCl_4$ and different amounts of tetraethyl orthosilicate were added into the F127 ethanolic solution dropwise and stirred vigorously at 40 °C for 30 min. Then, 1.8 ml distilled water was slowly added into the above homogenous mixture, and stirred for another 30 min, resulting a transparent sol solution. The as prepared solution was spin-coated at a spinning rate of 1500 rpm onto the FTO substrates (2 cm × 2 cm), which were thoroughly cleaned under sonication in acetone, ethanol and distilled water to eliminate any organic and water soluble impurities successively and dried in air beforehand. The spin coating procedure was repeated five times at room temperature, giving reproducible thin films with strong adhesion with the FTO surfaces. The as-deposited films were aged for 2 days with relative humidity at 60% under room temperature, then thermo polymerized at 100 °C for 1d. Finally, highly ordered mesoporous TiO_2-SiO_2 films were obtained by calcination at certain temperature with a heating a ramp of 1 °C min^{-1} under air atmosphere.

The obtained films are denoted as TS-x-y, where TS means the TiO_2-SiO_2 composites, x represents the weight percentages of SiO_2, y stands for the calcination temperature of the composite films. The samples with different compositions in a range from 5 to 10 wt% of SiO_2 were prepared by varying the mass of TEOS. The pure ordered mesoporous TiO_2 film was also prepared for comparison by the same method without addition of TEOS, named TS-0-y.

Electrodeposition of Pt on the ordered mesoporous TiO_2-SiO_2 films. Potentiostatic pulse electrodeposition was employed to depositing Pt on the ordered mesoporous TiO_2-SiO_2 films. In a typical experiment, rectangular potential pulses were used and electrodeposition was carried out in an solution of 0.5 mol L^{-1} H_2SO_4 and 0.05 mol L^{-1} H_2PtCl_6 through a typical three-electrode system, with ordered mesoporous TiO_2-SiO_2 films used as working electrode, a platinum foil as counter electrode, and a saturated calomel electrode (SCE) as reference electrode. During the pulsed electrodeposition, a potential of -0.3 V (vs. SCE) was applied for 1 s, followed by a potential of 0 V (vs. SCE) for 3 s. The number of consecutive pulses was 100, resulting in 100 s effective electrodeposition. The as-prepared Pt deposited TiO_2-SiO_2 films are denoted as Pt/TS-x-y.

Structure and property characterization

The powder X-ray diffraction (XRD) patterns were recorded by a Bruker D8 Advance diffractmeter using Cu Kα radiation (λ = 0.154056 nm). The field emission scanning electron microscopy (FE-SEM) images and elemental mapping images were obtained on a Hitachi S-4800 microscope to observe the surface and cross-section images of the film. Transmission electron microscopy (TEM, FEI Tecnai G2) operating at 200 kV was applied to characterize the morphology of the

mesoporous materials. Samples were scratched from the substrate, embedded into ethanol and ultrasonically dispersed before TEM observation. Fourier transforming infrared spectrum (FT-IR) was recorded on Nicolet NEXUS-670. The samples were mixed with KBr ratio of 1:100, grinded uniformly and pressed to small rounds by tablet presses before test.

Electrochemical and photo-electrochemical measurements were carried out in a quartz beaker (100 mL), using a conventional three-electrode system with Pt foil and saturated calomel electrode (SCE) as the counter and reference electrodes, respectively. The working electrode was prepared by encapsulating the FTO with insulating tape, exposing an area of 1 cm^2. The electrochemical and photo-electrochemical behaviors of the TiO_2-SiO_2 and Pt/TiO_2-SiO_2 electrodes were characterized by amperometric i-t curve and cyclic voltammetry techniques in 1.0 mol L^{-1} CH_3OH + 0.5 mol L^{-1} KOH aqueous solution with or without UV illumination. The scan rate of cyclic voltammetry was 20 mV s^{-1} in the potential range of −0.6 to 0.5 V (vs. SCE). An 8 W UV light was employed as the UV excitation source. All measurements were performed on a CHI 660C electrochemical workstation at 298 K.

Results and discussion

Fig.1 illustrates the facile fabrication process of ordered mesoporous TiO_2-SiO_2 films. At first, F127, $TiCl_4$ and TEOS co-assemble into nanorod micelles under stirring in the hydro-alcoholic solutions. The block copolymer F127 forms complexes with preformed precursor inorganic particles via weak coordination bonds and hydrogen bonds, resulting in the uniform dispersion of metal atoms throughout the nascent phase. Afterwards, the thin films were obtained reproducibly by spin-coating the homogeneous solution onto FTO substrate. During the solvent evaporation induced self-assembly (EISA) process, the micelles self-arrange into ordered thin film nanophase under the preferential evaporation of the solvent. After suffering from thermal polymerization and calcination to remove the template, highly ordered mesoporous transparent TiO_2-SiO_2 films with narrow mesopore size distribution can be synthesized at last.

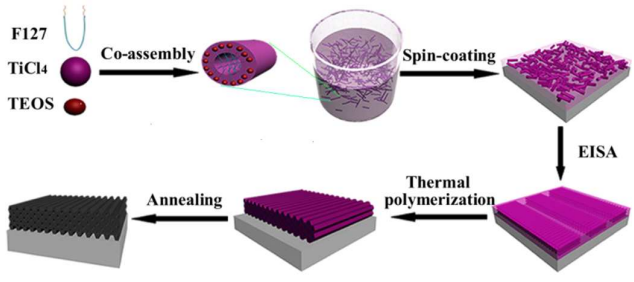

Fig.1. Schematic illustration of the formation process of highly ordered mesoporous TiO_2-SiO_2 films on the FTO substrate.

Effect of SiO_2 contents on ordered mesoporous TiO_2-SiO_2 films

In order to investigate the effect of SiO_2 contents on the ordered mesoporous structure and electrochemical as well as photo-electrochemical performance of the mesoporous TiO_2-SiO_2 and Pt/TiO_2-SiO_2 films, different amounts of tetraethyl orthosilicate were added to the sol with all the TiO_2-SiO_2 films finally calcined at 450 °C. Small-angle XRD measurements shown in Fig.2 (a) were conducted to study the mesoporous structural ordering of the TiO_2-SiO_2 films with different SiO_2 doping content. It is obvious that peak intensity of the TiO_2-SiO_2 composite films goes stronger as the SiO_2 content increases, indicating the better ordered structure. TS-7.5-450 and TS-10-450 films display two well-resolved peaks at 2θ around 0.7° and 1.7°, which can be indexed to the (10) and (20) Bragg reflections, respectively, implying the ordered 2D hexagonal symmetry with P6mm space group of TiO_2-SiO_2 films[37]. However, as for the pure TiO_2 film (TS-0-450), no obvious peaks appear. TS-5-450 shows only a weak peak, indicating the weak ordering of the film. The poor ordering of the TS-5-450 film might be ascribed to that small content of SiO_2 doping could not effectually prevent the excessive growth of TiO_2 nanoparticles during calcinations. From these comparisons we can get that moderate addition of tetraethyl orthosilicate in precursors can notably improve the mechanical strength and ordering of the mesoporous structures undergoing high temperature heat treatment.

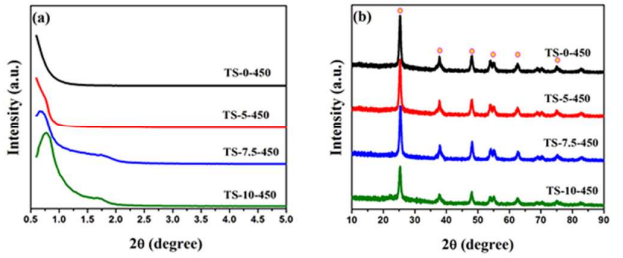

Fig.2. (a) Small-angle XRD and (b) wide-angle XRD patterns of ordered mesoporous TiO_2-SiO_2 films.

Wide-angle XRD patterns exhibit the crystalline phase of TiO_2-SiO_2 films, as illustrated in Fig.2 (b). Distinct diffraction peaks at 2θ of 25.3°, 37.8°, 48.0°, 55.1°, 62.7° and 75.2° are characteristic of the (101), (004), (200), (211), (204) and (215) lattice planes reflections of anatase (JCPDS Card 21-1272). There are no indications for either rutile or brookite phase, with all the patterns belonging to the anatase phase, which is considered to be an active phase in view of photocatalytic and photoelectrochemical properties due to its lower recombination rate of electron-hole pairs.[18, 27] And there are no diffraction peaks for SiO_2 as well, indicating that SiO_2 are amorphous. However, the peak intensity of TiO_2-SiO_2 films decreases with the increase of SiO_2 content, especially apparent for the TS-10-450 film, indicating that the crystallinity decreased. Meanwhile, as the silicon contents increase, the half-width of TiO_2 (101) peak becomes wider, suggesting the smaller crystallite size. Estimated from Scherrer equation ($D = k\lambda/\beta\cos\theta$), the average TiO_2 crystalline sizes in TiO_2-SiO_2 films (0~10%) are 14.6, 14.2, 13.6 and 12.8 nm, respectively, which might result from the existence of SiO_2 which helps to confine the growth of TiO_2 during heat treatment. The above results

reveal that the crystallinity becomes weaker and crystallite sizes of TiO_2 crystalline become smaller with the increasing of silicon content.

Fourier transforming infrared spectrum (FT-IR) of TS-7.5-450 was carried out to measure the functional groups and atomic compositions, shown in Fig.3. The spectrum shows hardly characteristic bands of organic groups,[38] indicating the efficient removal of F127 surfactant through heat treatment. Considering the fact that surfactant can absorb amount of light and thus have a competition with the catalyst in light absorption, complete elimination of F127 is of great importance for the following catalytic performance.[25] The peak around 3400 cm^{-1} belongs to the stretching vibrations of hydroxyl groups or adsorbed water, demonstrating the existence of abundant hydroxyl or water on the surface of TiO_2-SiO_2 films. What need mention is that the surface hydroxyl groups[39] and water[40], which can capture the photo-induced holes and thereafter generate strong active oxidizing species such as hydroxyl radicals, play an important role in heterogeneous photocatalysis. The band at 736 cm^{-1} corresponds to Si–O–Si stretching vibrations.[41] The peak at around 930 cm^{-1} can be assigned to the Si-O-Ti asymmetric stretching vibrations,[42] indicating the presence of chemical bonds linkages between TiO_2 and SiO_2 instead of a simple mixture. Under moderate hydrolysis and condensation rates of the titania and silica precursors during the co-assembly progress, a portion of TiO_x species can polymerize with surface Si-OH of silica to generate Ti-O-Si linkages,[43] which can enhance the surface acidity and subsequently adsorb more hydroxyl groups on the particle surface in turn.[44] Substitution of Si atom for Ti in the Ti-O matrix can effectively prevent the overgrowth and aggregation of TiO_2 particles, which will hence help to remain the ordered mesoporous structure. The results are well in accord with the above XRD patterns.

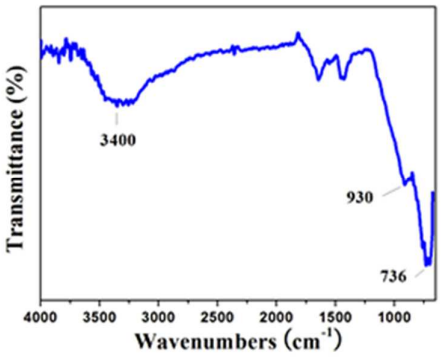

Fig.3. FT-IR spectrum of TS-7.5-450 ordered mesoporous film.

The FE-SEM images can intuitively demonstrate the ordered structure in details. The FE-SEM images of TiO_2-SiO_2 films obtained by varying silicon precursor ratios are shown in Fig.4. As observed in Fig.4 (a) and (b), the TS-0-450 film shows disordered pores and TS-5-450 film exemplifies the unobvious ordering mesoporous structure, which may be on account of the overgrowth of TiO_2 crystal particles during the high temperature heat treatment, accompanied with the mesoporous wall distorted or collapsed. Further increasing the SiO_2 doping content, the TS-7.5-450 film and TS-10-450 film possess highly ordered mesoporous structure over a large area, shown in Fig.4 (c) and (d). These results manifest that the higher content of SiO_2 precursor, the stronger confine effect of SiO_2 emerged to keep the TiO_2 crystal particles from overgrowth, which agrees with the above results. From the crack section part of later Fig.9 (a), we can see clearly that TiO_2 nanowires piece by piece stacked orderly along the same direction parallel to the supported substrate. Inset of Fig.4 (d) is the cross section of the TiO_2-SiO_2 film on FTO, indicating the thickness of the TiO_2-SiO_2 composite films is about 1.0 μm, which can be adjusted by controlling the spin-coating times.

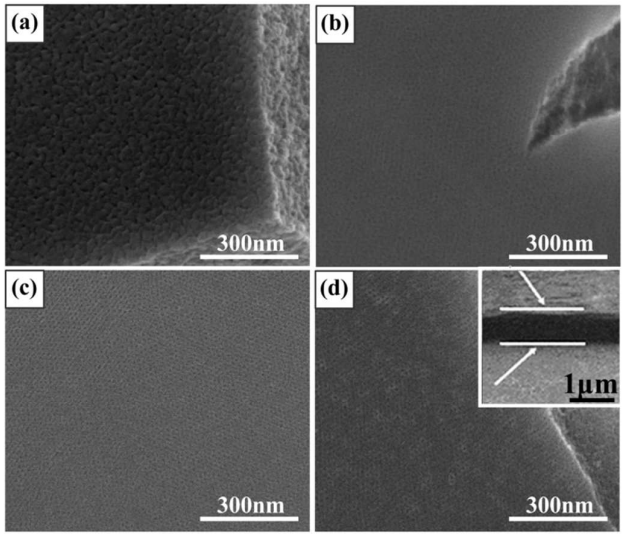

Fig.4. FE-SEM images of (a) TS-0-450, (b) TS-5-450, (c) TS-7.5-450, (d) TS-10-450 films. Inset image of (d) is the cross section SEM image of TiO_2-SiO_2 films.

We observed structural characterization through TEM imaging by scraping off the films and dispersing them in ethanol under sonication, and the images are shown in Fig.5. From Fig.5 (a) and (b), pure TiO_2 (TS-0-450) possesses the disordered structure and TiO_2 film doped with small content of SiO_2 (TS-5-450) shows a vague mesoporous structure. Nevertheless, in the case of TS-7.5-450 and TS-10-450 films, highly ordered mesostructure with large-domain regularity is illustrated in Fig.5 (c) and (d), in which the mesoporous channels are arranged straight and regular array parallel to each other, further indicating the well-ordered hexagonal arrays of mesopores with 2D channels. The moderate doping amount of SiO_2 can effectively confine the over growth of crystal particles and help to maintain the mesoporous structure undergoing the high temperature treatment, which is further consistent with results of the above XRD and FE-SEM results.

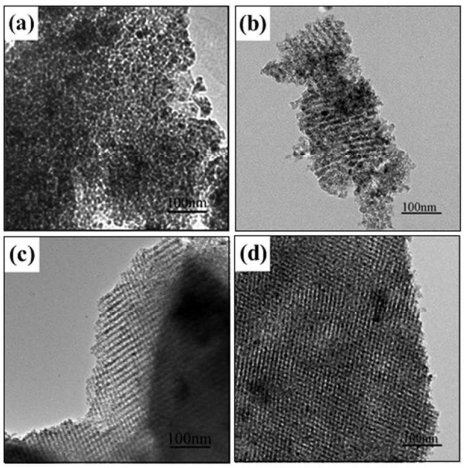

Fig.5. TEM images of (a) TS-0-450, (b) TS-5-450, (c) TS-7.5-450 and (d) TS-10-450 films.

Considering the above analysis, incorporation of SiO_2 can effectively protect the TiO_2 skeletons from crystal overgrowth via chemical bonds and remain the ordered mesostructure under calcinations to gain the better thermal stability, which can in turn increase the specific area and facilitate mass transportation of the composites, and enhance the catalytic performance at last.

To investigate the methanol oxidation properties, the common catalyst Pt was potentiostatic pulse electrodeposited on the ordered mesoporous TiO_2-SiO_2 film. The photoelectrochemical characteristics of the ordered mesoporous TiO_2-SiO_2 and Pt/TiO_2-SiO_2 films were measured by amperometric I–t curves and cyclic voltammetry in 1.0 mol L^{-1} CH_3OH + 0.5 mol L^{-1} KOH aqueous solution. Fig.6 is the photocurrent response of ordered mesoporous TiO_2-SiO_2 and Pt/TiO_2-SiO_2 films and as shown, all samples exhibit fast and reproducible photocurrent response. From Fig.6 (a), without UV illumination (before Light on), current density of TiO_2-SiO_2 films is only about 1 μA cm^{-2} whereas the values obtained under ultraviolet irradiation represent 100 times. Since TiO_2 is a wide band semiconductor, it has a poor electrical conductivity but upon illumination by UV, TiO_2 can get activated to generate electron–hole pairs, which will migrate and form photocurrent to counter electrode, thus increasing the current obviously. The current density of TS-5-450 under UV irradiation is 0.33 mA cm^{-2}, less than that of pure TiO_2, being 0.48 mA cm^{-2}. According to the above analysis, small content doped SiO_2 might not effectively control the growth of the TiO_2 crystal particles, resulting in ambiguous ordered structure formed in the film. Considering that SiO_2 has no photoelectric effect, addition of which leads to the decrease of the current instead. As doping content of SiO_2 increase, the current density under UV irradiation reaches to 0.54 mA cm^{-2} in the case of TS-7.5-450, with outstanding ordered mesoporous structure and excellent photoelectric effect performance at the same time. However, when doping SiO_2 content reaches to 10%, the current density declines (0.40 mA cm^{-2}) though TS-10-450 has highly ordered mesoporous framework. This indicates that over addition of SiO_2 will harm the photoelectric effect performance, for the bad conductivity of SiO_2 might do harm to the fast carriers transportation. To summarize, the improved separation of electron-hole pairs under ultraviolet irradiation can effectively compensate for the low electrical conductivity the TiO_2-SiO_2 films.

As shown in Fig.6 (b), photocurrent responses of all Pt/TiO_2-SiO_2 samples have accordingly increased compared with the TiO_2-SiO_2 films whether with or without UV illumination. While irradiated by UV, the current densities of film electrodes rise up to higher values with better photoelectric effect. The Pt/TiO_2-SiO_2 electrodes with doping SiO_2 content 0, 5, 7.5 and 10% have the current values of 0.60 mA cm^{-2}, 0.40 mA cm^{-2}, 0.71 mA cm^{-2} and 0.50 mA cm^{-2}, correspondingly. In particular, the result clearly demonstrates the superiority of the Pt/TS-7.5-450 film, declaring that proper SiO_2 doping content can enhance the photoelectric effect.

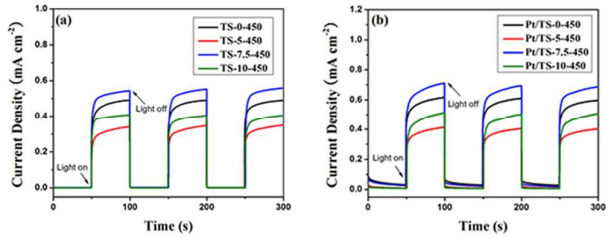

Fig.6. Photocurrent response of (a) ordered mesoporous TiO_2-SiO_2 films and (b) Pt/TiO_2-SiO_2 films with and without UV irradiation in the electrolyte of 1.0 mol L^{-1} CH_3OH + 0.5 mol L^{-1} KOH aqueous solution.

To further investigate the catalytic methanol oxidation performance of ordered mesoporous TiO_2-SiO_2 and Pt/TiO_2-SiO_2 films, cyclic voltammetry curves are shown in Fig.7. Little current response is observed for the TiO_2-SiO_2 films in the cyclic voltammetry without UV irradiation as a result of the poor conductivity of semiconductor, as shown in Fig.7 (a), which agrees to the photocurrent response curves. In Fig.7 (b), the current density of all TiO_2-SiO_2 films increase obviously as soon as they are exposed to UV. Electrons generated in TiO_2 transferring to the counter electrodes can bring about a current response. At the same time, photo-generated holes migrate to the surface of TiO_2-SiO_2 films and oxidize the abundant surface bound hydroxyl groups or water to generate •OH radicals, which have a strong oxidizing ability toward methanol.[19] However, the photocurrents in Fig. 7(b) from the methanol oxidation by holes together with their reaction products still need to be strengthened especially at lower potential.

After Pt was electrodeposited on the ordered mesoporous TiO_2-SiO_2 films, great difference appears. As shown in the Fig.7 (c), there are two methanol oxidation peaks at around -0.2V and -0.4V, which are derived from the excellent electrocatalysis of Pt due to the absence of UV illumination. The peak current densities of all Pt/TiO_2-SiO_2 samples is around 0.30 mA cm^{-2} and CV curves is almost coincident or close in the entire texted region, demonstrating that all the films have similar electrocatalytic ability for methanol oxidation. When the Pt/TiO_2-SiO_2 films are UV irradiated in Fig.7 (d), the current densities of all samples are much higher

than that of films without UV illumination as photogenerated electrons and holes in TiO_2 excited by irradiation can make for the photo-electrochemical methanol oxidation process. Meanwhile, Pt can somewhat increase TiO_2 photocurrent generation by acting as an electron sink for the photogenerated conduction band electrons and prohibiting the fast recombination of photogenerated electron-hole pairs. Among them, peak current density of Pt/TS-7.5-450 reaches to as high as 0.95 mA cm^{-2}, indicating the best performance for methanol oxidation by the electrocatalytic process as well as the additionally photo-assisted oxidation.[45]

In addition, compared with Fig.7 (c), peaks of Pt/TiO_2-SiO_2 films irradiated under UV in Fig.7 (d) turn to have slightly more positive potential positions accordingly. In the case of typical methanol electrooxidation in Fig.7 (c), the oxidation currents in the positive scan increase progressively with increase of potential and then decrease rapidly, which can be ascribed to the loss of active Pt sites such as intermediate species adsorption. When UV irradiation in Fig.7 (d), the photo generated holes and their reaction products (•OH) on TiO_2 contribute to the extra oxidation of the reactive intermediates to some extend.[45] As a result, the peak positions move to the more positive direction. Meanwhile, as the increase of SiO_2 doping contents, the peak potentials in both Fig.7 (c) and Fig.7 (d) move to the negative position, for the poor photoelectric effect and bad conductivity of SiO_2 have slightly bad effect on the photoelectric performance of the TiO_2-SiO_2 films. However, the effect to peak position is limited. [35, 37]

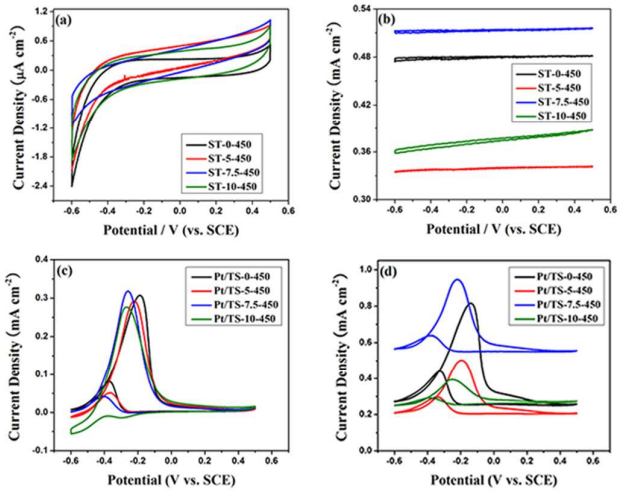

Fig.7. Cycle voltammetry curves of ordered mesoporous TiO_2-SiO_2 films (a) without UV irradiation and (b) with UV irradiation. Cycle voltammetry curves of Pt/TiO_2-SiO_2 films (c) without UV irradiation and (d) with UV irradiation. The electrolyte is 1.0 mol L^{-1} CH_3OH + 0.5 mol L^{-1} KOH aqueous solution with scan rate of 20 mV s^{-1}.

Effect of calcination temperatures on ordered mesoporous TiO_2-SiO_2 films

Based on the above analysis, it's obvious that the TiO_2-SiO_2 film with SiO_2 doping content being 7.5% may be an appropriate additive amount for Pt support, which have the molar ratio of SiO_2 to TiO_2 being 1:10, since it has the proper structure and performance at the same time. It's well known that degree of crystallinity could increase at a higher heat treatment temperature, leading to better catalytic effect. In order to investigate the effect of calcination temperature on ordering and catalytic performance of the TiO_2-SiO_2 and Pt/TiO_2-SiO_2 films, three kinds of ordered mesoporous TiO_2-SiO_2 films were prepared by adjusting the calcination temperature from 450 to 550 °C. The resulting composite films are labeled as TS-7.5-y (y represents for 450, 500, or 550 °C).

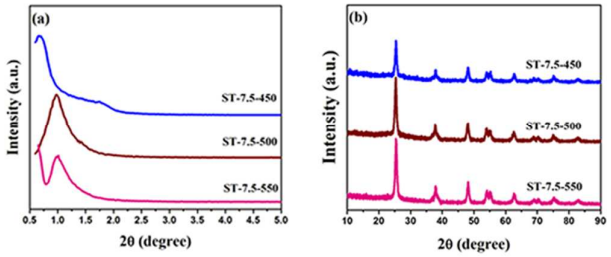

Fig.8. (a) Small-angle XRD and (b) wide-angle XRD patterns of ordered mesoporous TiO_2-SiO_2 films.

The growth progress of TiO_2 crystalline grains at high temperature undoubtedly has a great influence on the resulting mesoporous structure. We took XRD and FE-SEM to observe the characterization of ordered mesoporous TiO_2-SiO_2 films. As shown in Fig.8 (a), all samples display well-resolved diffraction peak, indicating that the ordering mesostructure of TiO_2-SiO_2 films can keep thermally stable at as high as 550 °C. However, the ordering of films decrease slightly as temperature rises. The ordering of mesoporous structure can be observed intuitively in the following FE-SEM images, shown in Fig.9. The ordered mesoporous structure can be observed clearly on all composite films, showing that addition of SiO_2 into TiO_2 framework can enhance the heat endurance of the mesoporous structure to 550 °C. However, TS-7.5-550 has a slight collapse compared to TS-7.5-450 and TS-7.5-500. In Fig.9 (d), elemental mapping image of TS-7.5-500 shows that SiO_2 has been uniformly incorporated into the TiO_2 framework, implying the homogeneous Ti-O-Si linkages. In other word, under the experiment conditions, no phase separation occurred during the sol-gel process. From the wide-angle XRD patterns in Fig.8 (b), we can find that the product is anatase TiO_2 under the three calcined temperature and stronger diffraction peaks are observed with the higher heat treat temperature, implying the better crystallinity.

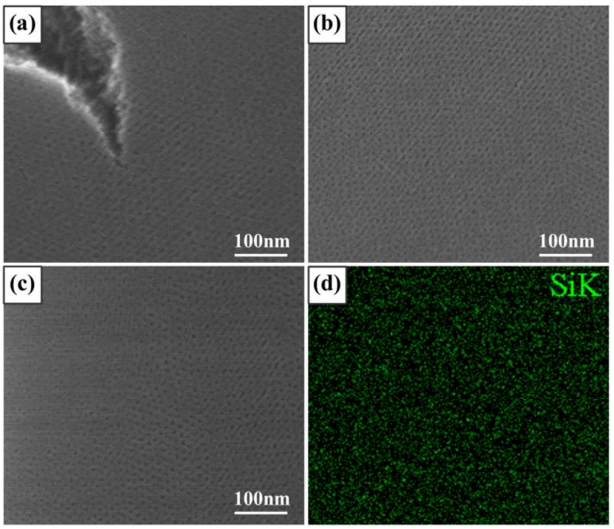

Fig.9. FE-SEM images of (a) TS-7.5-450, (b) TS-7.5-500 and (c) TS-7.5-550 films and (d) Si elemental mapping image of TS-7.5-500 film.

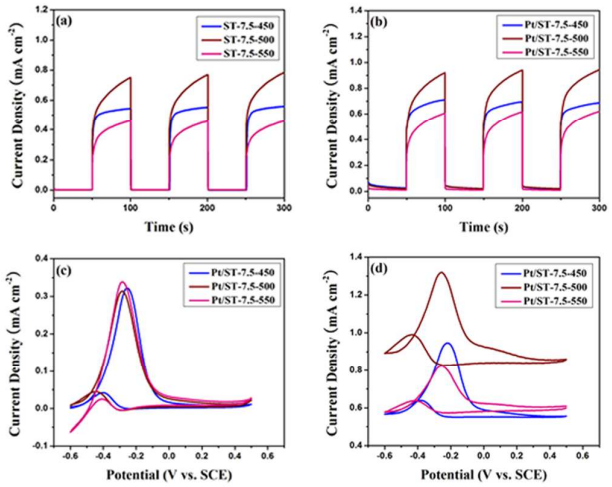

Fig.10. Photocurrent response of (a) ordered mesoporous TiO_2-SiO_2 films and (b) Pt/TiO_2-SiO_2 films with and without UV irradiation. Cycle voltammetry curves of Pt/TiO_2-SiO_2 films (c) without UV irradiation and (d) with UV irradiation. The electrolyte is 1.0 mol L^{-1} CH_3OH + 0.5 mol L^{-1} KOH aqueous solution with scan rate of 20 mV s^{-1}.

Photocurrent response of ordered mesoporous TiO_2-SiO_2 films carbonized at different temperature and corresponding Pt/TiO_2-SiO_2 films is shown in Fig.10 (a) and (b). Illuminated by UV in Fig.10 (a), the current densities of TiO_2-SiO_2 films rise up at once with the values being 0.54 mA cm^{-2}, 0.72 mA cm^{-2} and 0.45 mA cm^{-2}, respectively. Obviously, TS-7.5-500 has the highest current densities out of the three TiO_2-SiO_2 films. Upon the textural analysts, we can conclude that the best photoelectric effect comes from its better crystallinity degree than TS-7.5-450 and proper ordered mesoporous structure than TS-7.5-550. As shown in Fig.10 (b), current densities and photocurrents of all Pt/TiO_2-SiO_2 films have increased in the entire potential region than that of the TiO_2-SiO_2 films, accordingly, suggesting the better photoelectric effect. 500 °C is a proper heat treat temperature as Pt/TS-7.5-500 shows the best photoelectric response, which is in accord with results of Fig.10 (a).

Cyclic voltammetry of Pt/TiO_2-SiO_2 films was employed to examine the photoelectric catalytic methanol oxidation performance. Without UV irradiation in Fig.10 (c), two peaks appear on account of the electrochemical methanol oxidation. All samples show almost the same peak current density, about 0.31 mA cm^{-2} at around -0.2V, indicating the comparable amount of electrodeposited Pt and electric catalytic methanol oxidation ability of Pt/TiO_2-SiO_2 films. When irradiated under UV in Fig.10 (d), current densities arise in the whole testing potential region. The peak current densities of composites heated at 450, 500 and 550 °C are 0.95 mA cm^{-2}, 1.35 mA cm^{-2} and 0.85 mA cm^{-2}, respectively, showing the preferable photoelectric synergic catalysis performance for methanol oxidation. Notably, the poor crystallinity degree of TS-7.5-450 and the less ordered mesoporous structure as well as the larger crystal size of TS-7.5-550 make their photocurrent and peak current density of CV less than that of TS-7.5-500, which has the proper relation between ordered mesoporous structure and electroconductivity.

Generally, small gain size and large specific area mean more active sites and consequently better catalytic activity of catalyst. For TiO_2 particles, the average transfer time of photo-generated electrons from crystal center to the surface can be estimated by the following formula[47],

$$\tau = r^2/\pi^2 D$$

Where *r* is the radius of TiO_2 particles, *D* means diffusion coefficient of charge carriers. According to the equation, electron transfer time is proportional to the square of particle size. As a result, smaller crystal size can significantly decrease the transfer time while oversized particles will bring about less electrons moving to the surface and correspondingly high recombination rate of electrons and holes. In the case of TiO_2-SiO_2 composite films, proper addition of SiO_2 can not only effectively confine the overgrowth of TiO_2 grains by formation of chemical bridges, but also make it gain high crystallinity without destroying the ordered structure after heat treatment at higher treatment, which can subsequently promote photoelectric performance. Moreover, the abundant hydroxyl and absorbed water on the surface of TiO_2-SiO_2 films is in favour of capturing the photo-induced holes, helping to increase the photoelectric response as well. All the above analysis declares that doping of SiO_2 makes the resulting films with desirable performance.

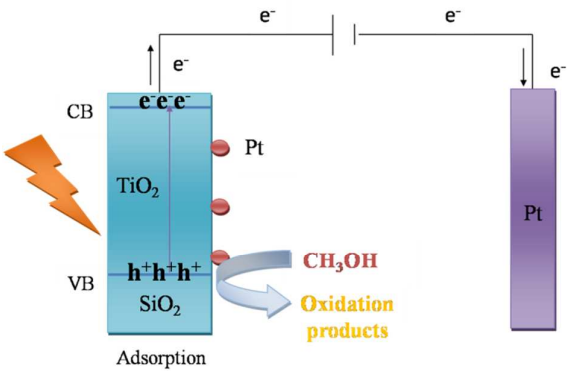

Fig.11. Schematic diagram of photo-assisted electrocatalytic methanol oxidation on ordered mesoporous Pt/TiO_2-SiO_2 films with UV irradiation.

A possible mechanism for methanol photoelectrocatalysis on the Pt/TiO_2-SiO_2 film under UV illumination is on account of the special synergetic photoelectric effects between Pt and TiO_2-SiO_2 films. As shown in Fig.11, with UV illumination, electrons are excited and leapt into the conduction band, and leave behind holes in the valence band. Under the working environment, photogenerated electrons would transfer to the Pt electrode and take part in reduction reaction there, which significantly increase the current density in the whole potential region. The left photogenerated holes together with their oxidizing reactive intermediate with the solution possess high oxidizing ability, [46] leading to the additionally photo-assisted electrocatalytic methanol oxidation. The special photoelectric synergetic catalytic oxidation for methanol between TiO_2-SiO_2 films and Pt makes the Pt/TiO_2-SiO_2 films giving superior performance. Additionally, compact interactions between TiO_2 and Pt make for prohibiting the fast recombination of photogenerated carriers, by forming metal/semiconductor nanoheterojunctions. Above all, under UV irradiation the ordered mesoporous TiO_2-SiO_2 films serve as the Pt support and act as the additional photo-induced catalyst for methanol oxidation at the same time. The greatly promoted electrocatalytic activity for methanol oxidation of Pt/TiO_2-SiO_2 films, which combines increased active sites of ordered mesoporous structure, enhanced crystallization of the TiO_2 network and preferable synergetic catalytic effect between Pt and holes, brings it great potential in developing new generation DMFCs.

Conclusions

In present work, we have synthesized SiO_2 incorporated ordered mesoporous TiO_2 composite films and investigated their performance as the support materials for Pt in methanol oxidation. We find that the introduction of 7.5% SiO_2 into TiO_2 network structures effectively hinders the overgrowth of the anatase phase crystal and prevents the TiO_2 framework from shrinkage, which manages to keep the ordered mesostructure in TiO_2 films even after 550 °C heat treatment. What is more, the Pt/TiO_2-SiO_2 nanocomposite electrode with 7.5 wt % of SiO_2 and 500°C calcination temperature can obviously enhances the electron-hole separation efficiency and demonstrate superior photoelectrocatalytic performance for methanol oxidation due to the special synergetic effects between Pt and holes under UV illumination, which can provide a positive reference to design new generation DMFCs.

Acknowledgements

The authors appreciate the financial support from the National Natural Science Foundation of China (51372115 and 51402150), Natural Science Foundation of Jiangsu Province (BK20130737) and A Project Funded by the Priority Academic Program Development of Jiangsu Higher Education Institutions (PAPD).

Notes and references

1 Y. Zhang, R. Zhu, Y. Cui, J. Zhong, X. Zhang and J. Chen, *Nanotechnology*, 2014, **25**, 135607-135614.
2 F. Ye, H. Liu, Y. Feng, J. Li, X. Wang and J. Yang, *Electrochim. Acta*, 2014, **117**, 480-485.
3 C. S. Sharma, R. Awasthi, R. N. Singh and A. S. K. Sinha, *Phys.Chem. Chem. Phys.*, 2013, **15**, 20333-20344.
4 L. A. Estudillo-Wong, A. M. Vargas-Gòmeza, E. M. Arce-Estradab and A. Manzo-Robledoa, *Electrochim. Acta*, 2013, **112**, 164-170.
5 Y. Cheng and S. P. Jiang, *Electrochim. Acta*, 2013, **99**, 124-132.
6 S. Sharma and B. G. Pollet, *J. Power Sources*, 2012, **208**, 96-119.
7 S. Y. Huang, P. Ganesan, S. Park and B. N. Popov, *J. Am. Chem. Soc.*, 2009, **131**, 13898-13899.
8 Y. Qu, Y. Gao, F. Kong, S. Zhang, L. Du and G. Yin, *Int. J. Hydrogen Energy*, 2013, **38**, 12310-12317.
9 A. Leelavathi, G. Madras and N. Ravishankar, *J. Am. Chem. Soc.*, 2014, **136**, 14445−14455.
10 C. Pandiyarajan, A. Pandikumar and R. Ramaraj, *Nanotechnology*, 2013, **24**, 435401-435409.
11 A. S. Polo, M. C. Santos, R. F. B. de Souza and W. A. Alves, *J. Power Sources*, 2011, **196**, 872-876.
12 R. Ganesan and J. S. Lee, *J. Power Sources*, 2006, **157**, 217-221.
13 S. Jayaraman, T. F. Jaramillo, S. H. Baeck and E. W. McFarland, *J. Phys. Chem. B*, 2005, **109**, 22958-22966.
14 C. Y. Su, Y. C. Hsueh, C. C. Kei, C. T. Lin and T. P. Perng, *J. Phys. Chem. C*, 2013, **117**, 11610-11618.
15 Y. Zhao, F. Wang, J. Tian, X. Yang and L. Zhan, *Electrochim. Acta*, 2010, **55**, 8998-9003.
16 S. Yu, Q. Liu, W. Yang, K. Han, Z. Wang and H. Zhu, *Electrochim. Acta*, 2013, **94**, 245-251.
17 M. Gustavsson, H. Ekstr¨omc, P. Hanarp, L. Eurenius, G. Lindbergh, E. Olsson and B. Kasemo, *J. Power Sources*, 2007, **163**, 671-678.
18 J. B. Joo, Q. Zhang, I. Lee, M. Dahl, F. Zaera and Y. Yin, *Adv. Funct. Mater.*, 2012, **22**, 166-174.
19 A. A. Ismail, D. W. Bahnemann, L. Robben, V. Yarovyi and M. Wark, *Chem. Mater.*, 2010, **22**, 108-116.
20 S. Gardin, R. Signorini, A. Pistore, G. D. Giustina, G. Brusatin, M. Guglielmi and R. Bozio, *J. Phys. Chem. C*, 2010, **114**, 7646-7652.
21 J. Yang, W. Liao, Y. Liu, M. Murugananthan and Y. Zhang, *Electrochim. Acta,* 2014, **144**, 7-15.

22 C. V. Subban, Q. Zhou, A. Hu, T. E. Moylan, F. T. Wagner and F. J. DiSalvo, *J. Am. Chem. Soc.*, 2010, **132**, 17531-17536.
23 A. Naldoni, M. D'Arienzo, M. Altomare, M. Marelli, R. Scotti, F. Morazzoni, E. Selli and V. D. Santo, *Appl. Catal., B: Environ.*, 2013, **130-131**, 239-248.
24 C. Wang, F. Jiang, R. Yue, H. Wang and Y. Du, *J. Solid State Electrochem.*, 2014, **2**, 515-522.
25 Y. Yang, F. Su, S. Zhang, W. Guo, X. Yuan and Y. Guo, *Colloids Surf. A: Physicochem. Eng. Aspects*, 2012, **415**, 399-405.
26 X. Meng, T. Wang, L. Liu, S. Ouyang, P. Li, H. Hu, T. Kako, H. Iwai, A. Tanaka and J. Ye, *Angew. Chem. Int. Ed*., 2014, **126**, 1-6.
27 A. A. Ismail and D. W. Bahnemann, *Green Chem*., 2011, **13**, 428-435.
28 M. Bidaoui, C. Especel, N. Bouchenafa-Saib, D. Duprez, O. Mohammedi and S. Royer, *Appl. Catal., A: General*, 2012, **445-446**, 14-25.
29 W. N. Wang, J. Park and P. Biswas, *Catal. Sci. Technol.*, 2011, **1**, 593-600.
30 H. Hou, L. Wang, F. Gao, G. Wei, J. Zheng, B. Tang and W. Yang, *RSC Adv*., 2014, **4**, 19939-19944.
31 X. Gao and I. E. Wachs, *Catal. Today*, 1999, **51**, 233-254.
32 T. Sreethawong and S. Yoshikawa, *Chem.l Eng. J.*, 2012, **197**, 272-282.
33 C. X. Lei, H. Zhou, C. Wang and Z. D. Feng, *Electrochim. Acta*, 2013, **87**, 245-249.
34 J. Wang, H. Li, H. Li, C. Zou, H. Wang and D. Li, *ACS Appl. Mater. Interfaces*, 2014, **6**, 1623-1631.
35 S. Wu, J. He, J. Zhou, T. Wang, Y. Guo, J. Zhao and X. Ding, *J. Mater. Chem.*, 2011, **21**, 2852-2854.
36 Y. Guo, J. He, S. Wu, T. Wang, G. Li, Y. Hu, H. Xue, X. Sun, J. Tang and M. Liu, *J. Power Sources*, 2012, **208**, 58-66.
37 T. Wang, J. Tang, S. Wu, X. Fan and J. He, *J. Power Sources*, 2014, **248**, 510-516.
38 J. Zhong, S. Liang, C. Xu, H. Wang and Y. Cheng, *Microporous Mesoporous Mater.*, 2012, **150**, 25-31.
39 X. Chen, X. Wang and X. Fu, *Energy Environ. Sci.*, 2009, **2**, 872-877.
40 A.Yamakata, T. Ishibashi and H. Onishi, *J. Phys. Chem. B*, 2003, **107**, 9820-9823.
41 Jun Ren, Zhong Li, Shusen Liu, Yanling Xing and Kechang Xie, *Catal. Lett.*, 2008, **124**, 185-194.
42 J. J. Zhang, Z. Wei, T. Huang, Z. L. Liu and A. S. Yu, *J. Mater. Chem. A*, 2013, **1**, 7360-7369.
43 H. S. Kibombo, R. Peng, S. Rasalingam and R. T. Koodali, *Catal. Sci. Technol.*, 2012, **2**, 1737-1766.
44 K. Qi, X. Chen, Y. Liu, J. H. Xin, C. L. Mak and W. A. Daoud, *J. Mater. Chem.*, 2007, **17**, 3504-3508.
45 C. Jia, H. Yin, H. Ma, R. Wang, X. Ge, A. Zhou, X. Xu and Y. Ding, *J. Phys. Chem. C*, 2009, **113**, 16138-16143.
46 C. Zhai, M. Zhu, D. Bin, H. Wang, Y. Du, C. Wang and P. Yang, *ACS Appl. Mater. Interfaces*, 2014, **6**, 17753−17761.
47 D. E. Skinner, D. P. Colombo, Jr., J. J. Cavaleri and R. M. Bowman, *J. Phys. Chem.*, 1995, **99**, 7853-7856.